Enhancing spin-photon coupling with a micromagnet

Xin-Lei Hei, Xing-Liang Dong, Jia-Qiang Chen, Cai-Peng Shen, Yi-Fan Qiao, and Peng-Bo Li [*]
Shaanxi Province Key Laboratory of Quantum Information and Quantum Optoelectronic Devices,
School of Physics, Xi'an Jiaotong University, Xi'an 710049, China

Hybrid quantum systems involving solid-state spins and superconducting microwave cavities play a crucial role in quantum science and technology, but improving the spin-photon coupling at the single quantum level remains challenging in such systems. Here, we propose a simple technique to strongly couple a single solid-state spin to the microwave photons in a superconducting coplanar waveguide cavity via a magnetic microsphere. We show that strong coupling at the single spin level can be realized by virtual magnonic excitations of a nearby micromagnet. The spin-photon coupling strength can be enhanced up to typically 4 orders of magnitude larger than that without the use of the micromagnet. This work can find applications in quantum information processing with strongly coupled solid-state spin-photonic systems.

I. INTRODUCTION

Hybrid quantum architectures based on degrees of freedom of completely different nature have attracted much attention over recent years [1–22], due to a variety of applications in quantum technologies such as quantum networks [23], information processing [13,24], and sensing [25]. The interactions between solid-state spins and microwave photons play a central role in hybrid quantum systems [17–22], which associate the solid-state spins as quantum memories [26] and the photons as quantum information carriers [27]. Besides, they can be useful for fundamental investigation in quantum mechanics, solid-state physics, and quantum optics, which provide useful platforms and tools to deepen the research of currently unexploited quantum physics [28,29].

To construct hybrid solid-state platforms, color centers in diamond are often employed. For example, nitrogen-vacancy (NV) centers, one of the excellent color centers with long coherence time and stable triplet ground states [30–36], are frequently used for quantum storage [26] and sensing [37,38]. While the realization of strong coupling is difficult due to the large mismatch between the spatial extension of free-space photons and typical spins, the solid-state spins can strongly couple to superconducting coplanar waveguide (CPW) resonators [17,18,39], similar to cavity quantum electrodynamics with atoms [40]. However, current experiments in hybrid systems often involve spin ensembles rather than single spins [18,22,41,42], since the single spin-photon coupling strength is just around 10 Hz, which is far from the strong coupling regime [13,28].

Here, we propose a feasible scheme to realize the strong spin-photon coupling at the single quantum level via virtual excitations of magnons in a micromagnet. Magnons, the energy quanta of spin waves, play an essential role in quantum

information processing and quantum sensing [43–48], with different types of magnets such as sphere magnets [49–59], film layer magnets [60–66], and cylinder magnets [67]. Thanks to the small mode volume and high spin density of the Kittel mode in a sphere micromagnet, it can focus the field energy to enable the strong spin-magnon interaction [68]. Therefore, the Kittel mode in the sphere magnet is frequently used in the magnon-cavity coupling system to achieve the strong coupling between magnons and microwave cavity photons [41,47,69–76]. The nanoscale micromagnet, yttrium iron garnet (YIG) sphere, considered in this work is well matched with the NV spins and CPW cavities and is very crucial to the strong interactions among the three subsystems. We consider efficient coupling of magnonic excitations to a single NV spin and a CPW cavity. We show that, even when the Kittel mode is only virtually populated, the magnon-mediated interaction between the NV spin and the microwave cavity mode can be modified significantly. The induced spin-photon coupling strength can be enhanced up to typically 4 orders of magnitude larger than that in the absence of the micromagnet. This regime may provide a powerful tool for applications of quantum information processing based on strong spin-photon interactions at the single quantum level.

II. DESCRIPTION OF THE SYSTEM

A. The setup

As illustrated in Fig. 1(a), we consider a hybrid tripartite system where a spherical micromagnet with radius R is magnetically coupled to a NV center and a CPW resonator simultaneously. Here, the magnetic microsphere is a YIG sphere. The NV center is placed above the microsphere, which is close to the surface of the CPW resonator.

The magnetic microsphere supports spin waves, which always exist in the ferrimagnetic or antiferromagnetic materials in the low-energy limit. The spin wave in a magnetic
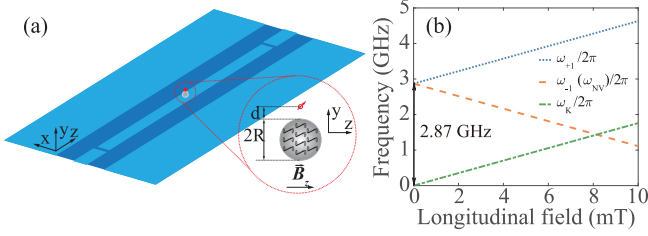
---

[*]lipengbo@mail.xjtu.edu.cn

FIG. 1. (a) Schematic of the NV center (red circle with arrow) coupled to a CPW cavity (blue field) via a YIG sphere (gray). (b) Frequency split of the NV center spin states and the resonant frequency of the Kittel mode changed with the longitudinal magnetic field.

microsphere can be quantized by the dipolar, isotropic, and magnetostatic approximations [58], with magnons as the quanta. In our setup, only the Kittel mode in the YIG sphere is considered, where all the spins in the magnetic sphere precess in phase and with the same amplitude [72]. The Hamiltonian of the Kittel mode (with the destruction operator $\hat{s}_K$) can be expressed as

$$\hat{H}_K = \hbar \omega_K \hat{s}_K^\dagger \hat{s}_K. \qquad (1)$$

Here, the frequency $\omega_K = |\gamma| B_z$ is controlled by the external magnetic field, with the gyromagnetic ratio $\gamma = -1.76 \times 10^{11} \text{ T}^{-1} \text{ s}^{-1}$.

For the NV center, the spin-triplet $S = 1$ ground states $\{|0\rangle, |\pm 1\rangle\}$ are the eigenstates of the spin operator $\hat{S}_z$, with $\hat{S}_z |i\rangle = i |i\rangle$ and $i = 0$ and ± 1. In the presence of the external magnetic field $\vec{B}_z$ oriented along the NV symmetry axis [31,32,34,77,78], the degeneracy of the states $|\pm 1\rangle$ are split via the Zeeman effect. Taking $|0\rangle$ as the energy reference, the Hamiltonian of the NV center can be expressed as

$$\hat{H}_{NV} = \hbar \sum_{i=\pm 1} \omega_i |i\rangle\langle i|, \qquad (2)$$

with $\omega_{\pm 1} = D_0 \pm |\gamma| B_z$ and the zero-field-splitting $D_0 = 2\pi \times 2.87$ GHz. With proper magnetic fields, we can choose the states $|0\rangle$ and $|-1\rangle$ as a spin qubit, which are selected to be resonant with the magnon mode. The Hamiltonian of the NV center can be simplified by

$$\hat{H}_{NV} = \frac{\hbar}{2} \omega_{NV} \hat{\sigma}_z, \qquad (3)$$

where we define the frequency as $\omega_{NV} \equiv \omega_{-1}$ and the spin operator as $\hat{\sigma}_z \equiv |-1\rangle\langle -1| - |0\rangle\langle 0|$. The state $|+1\rangle$ can be safely excluded due to its off-resonance with the Kittel mode.

The CPW resonator is a one-dimensional resonator whose frequency ω_C is related to the length of the transmission line segment. The electron oscillating in the line cavity creates a variational electromagnetic field, which can be quantized and interacts with other devices [71,76,79–81]. The corresponding Hamiltonian of photons in the CPW resonator can be written as

$$\hat{H}_C = \hbar \omega_C \hat{a}^\dagger \hat{a}, \qquad (4)$$

where $\hat{a}$ is the annihilation operator of the photon mode. The photon frequency is designed to match the frequencies of magnons and spins. That means, in this setup, the frequencies of the three individual systems are equivalent.

B. Interactions between spins and magnons

We now consider the quantization of the magnetic field induced by the magnetic sphere. This magnetic field exists both inside and outside the micromagnet. Here, we focus on the latter because of the location of spin qubit. From classical electrodynamics, the magnetic field of a magnetic sphere with the magnetization $\vec{M}$ can be expressed as

$$\vec{B}_m(\vec{r}) = \mu_0 R^3 / (3r^3) \{3(\vec{M} \cdot \vec{r}) \vec{r} / r^2 - \vec{M}\}, \qquad (5)$$

where $\mu_0 = 4\pi \times 10^{-7}$ T m/A is the vacuum permeability, R is the radius of the YIG sphere, and $\vec{r} = (r, \theta, \phi)$ is the position vector relative to the center of the magnetic sphere. After quantizing the spin wave, the corresponding magnetization operator $\hat{\vec{M}}$ of the Kittel mode is

$$\hat{\vec{M}} = M_K (\vec{m}_K \hat{s}_K + \vec{m}_K^* \hat{s}_K^\dagger), \qquad (6)$$

where $M_K = \sqrt{\hbar |\gamma| M_s / 2V}$ is the zero-point magnetization, M_s is the saturation magnetization, and V is the volume. Meanwhile, we define the Kittel mode function as $\vec{m}_K = \vec{e}_x + i \vec{e}_y$ with the unit coordinate vectors $\vec{e}_x$ and $\vec{e}_y$ (see more details in Appendix A). Remarkably, there is no z component in the mode function. From the above discussion, we can get the quantized magnetic field $\hat{\vec{B}}_m$ as

$$\hat{\vec{B}}_m(\vec{r}) = \frac{\mu_0 R^3 M_K}{3r^3} \{[(3C_\theta^2 - 1)\hat{X} + 3S_\theta C_\theta \hat{P}]\vec{e}_x$$
$$+ [3S_\theta C_\theta \hat{X} + (3S_\theta^2 - 1)\hat{P}]\vec{e}_y\}, \qquad (7)$$

where we define $C_\theta = \cos\theta$, $S_\theta = \sin\theta$, $\hat{X} = \hat{s}_K + \hat{s}_K^\dagger$, and $\hat{P} = i(\hat{s}_K - \hat{s}_K^\dagger)$ for convenience.

We then consider the interaction between the spin qubit and the Kittel mode in the micromagnet. When a magnetic dipole is placed in a magnetic field, it experiences a torque which tends to line it up parallel to the field. The Hamiltonian associated with this torque can be naturally written as

$$\hat{H}_{N-K} = -\frac{g_e \mu_B}{\hbar} \hat{\vec{B}}_m \cdot \hat{\vec{S}}, \qquad (8)$$

with the electronic spin Landé factor g_e, the Bohr magneton μ_B, and the spin operator $\hat{\vec{S}} = (\hat{S}_x, \hat{S}_y, \hat{S}_z)$. In this work, we define the corresponding components of the spin operator as $\hat{S}_x = \hbar(|-1\rangle\langle 0| + |0\rangle\langle -1|)/2$, $\hat{S}_y = \hbar(|-1\rangle\langle 0| - |0\rangle\langle -1|)/2i$. Assuming that the coupling strength is smaller than the resonance frequency, the spin-magnon interaction under the rotation-wave approximation can be described by

$$\hat{H}_{N-K} = -\hbar g(\hat{s}_K \hat{\sigma}^+ + \text{H.c.}), \qquad (9)$$

where the spin operators are $\hat{\sigma}^+ = |-1\rangle\langle 0|$ and $\hat{\sigma}^- = |0\rangle\langle -1|$. And the corresponding spin-magnon coupling strength is expressed as

$$g = \sqrt{\frac{|\gamma| M_s}{12\pi\hbar}} \frac{g_e \mu_0 \mu_B R^{3/2}}{(R+d)^3}, \qquad (10)$$

where the distance between the spin qubit and the surface of the magnetic sphere is $d = r - R$ [see Fig. 1(a)]. The coupling strength is proportional to the square root of the micromagnet volume with $d > R$, while the coupling strength decreases slowly with $R > d$. In Figs. 2(a) and 2(b), we show the dependence of the spin-magnon coupling as a function of R and
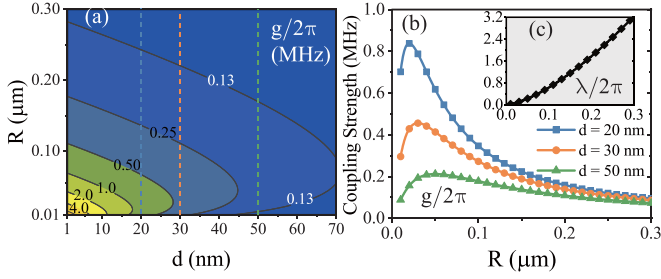
FIG. 2. (a) and (b) The coupling strength $g/2\pi$ between the individual NV center spin qubit and the Kittel mode in the YIG sphere versus the distance d and the radius R. (c) The coupling strength $\lambda/2\pi$ between the CPW resonator photon and the Kittel mode in the YIG sphere versus the radius R.

d. The coupling rate keeps reducing with the increase of d. While it increases with the growth of R until the maximum. From the numerical result we find that if we choose the YIG sphere with $R \sim 50$ nm and the distance $d \sim 10$ nm, then the coupling strength is about ~ 1 MHz.

C. Interactions between photons and magnons

We consider the quantizing form of the magnetic field generated by the CPW resonator. For the single mode, the magnetic field operator is

$$\hat{\vec{B}}_c = \vec{b}_{\text{tr}}(x, y)(\hat{a} + \hat{a}^\dagger)/\sqrt{2}. \tag{11}$$

Here, the mode function $\vec{b}_{\text{tr}}(x, y)$ varies strongly in space depending on the CPW resonator geometry. To obtain the stronger interaction, the magnetic sphere is in close proximity to the surface of the CPW resonator. Then the mode function depends on the radius of the sphere $[\vec{b}_{\text{tr}}(R)]$. From the discussion in Sec. II A, the radius is about tens of nanometers, which is less than the width of the CPW resonator ($\sim 1 \mu$m). Therefore, the variation of the mode function depending on the radius can be ignored and $\vec{b}_{\text{tr}}(R)$ acts as an estimated constant ranging from 35 to 40 μG.

We then expound the magnetic interaction between the CPW resonator and the micromagnet. The classical exchange energy of a magnetic dipole with the magnetic moment $\vec{m}$ in a uniform magnetic field $\vec{B}_c$ is $U = -\vec{m} \cdot \vec{B}_c$. For a uniformly magnetized sphere, we treat it as a magnetic dipole with $\vec{m} = V\vec{M}$. After replacing the classical quantity with the magnetization operator $\hat{\vec{M}}$ and the magnetic field operator $\hat{\vec{B}}_c$ in the expression above, the photon-magnon interaction Hamiltonian is

$$\hat{H}_{C-K} = -\hbar\lambda(\hat{s}_K + \hat{s}_K^\dagger)(\hat{a} + \hat{a}^\dagger).$$

Here, the homologous coupling strength is defined as

$$\lambda = \sqrt{\frac{\pi|\gamma|M_s}{3\hbar}} b_x(R)R^{3/2}. \tag{12}$$

We ignore the y component of $\vec{b}_{\text{tr}}(R)$, since the magnetic field is parallel to the x axis. Then, the photon-magnon coupling strength λ can be enhanced to around 1 MHz with a proper geometrical size of the magnetic microsphere [see Fig. 2(c)]. Under the rotating-wave approximation, we can get

the photon-magnon interaction Hamiltonian

$$\hat{H}_{C-K} = -\hbar\lambda(\hat{s}_K^\dagger\hat{a} + \text{H.c.}). \tag{13}$$

III. REALISTIC CONSIDERATION AND EXPERIMENTAL PARAMETERS

From the above discussion, we can obtain the total Hamiltonian of the hybrid spin-magnon-photon system, which can be expressed as

$$\begin{aligned}\hat{H} = \;& \hbar\omega_C\hat{a}^\dagger\hat{a} + \hbar\omega_K\hat{s}_K^\dagger\hat{s}_K + \tfrac{1}{2}\hbar\omega_{\text{NV}}\hat{\sigma}_z \\ & - \hbar g(\hat{s}_K\hat{\sigma}^+ + \text{H.c.}) - \hbar\lambda(\hat{s}_K^\dagger\hat{a} + \text{H.c.}),\end{aligned} \tag{14}$$

where the first three terms correspond to the free Hamiltonian from Eqs. (1), (3), and (4), and the last two terms describe two interactions: one between the Kittel mode and the NV center spin from Eq. (9), and the other between the Kittel mode and the photon in the CPW resonator from Eq. (13). As the Kittel mode is coupled both to the spin qubit and the CPW resonator photon, it is possible for it to work as a quantum interface between the spin qubit and the CPW resonator.

We now discuss the dynamics of the system in a realistic situation. In this case, we take into account the dephasing of the NV center spin (γ_s), the decays of the Kittel mode (γ_m), and the CPW resonator (κ). As a result, the master equation of the total system can be expressed as

$$\dot{\hat{\rho}}(t) = -i/\hbar[\hat{H}, \hat{\rho}] + \mathcal{L}[\hat{\rho}], \tag{15}$$

where $\hat{\rho}$ is the density operator. The last term in above equation is given by

$$\mathcal{L}[\hat{\rho}] = \gamma_s\mathcal{D}[\hat{\sigma}_z]\hat{\rho} + \sum_j\{(\bar{n}_j + 1)\Gamma_j\mathcal{D}[\hat{o}_j]\hat{\rho} + \bar{n}_j\Gamma_j\mathcal{D}[\hat{o}_j^\dagger]\hat{\rho}\}. \tag{16}$$

For compactness we define $\{\Gamma_m, \Gamma_p\} \equiv \{\gamma_m, \kappa\}$, $\{\hat{o}_m, \hat{o}_p\} \equiv \{\hat{s}_K, \hat{a}\}$, and $\mathcal{D}[\hat{o}]\hat{\rho} \equiv \hat{o}\hat{\rho}\hat{o}^\dagger - \{\hat{o}^\dagger\hat{o}, \hat{\rho}\}/2$. Here, we have introduced the thermal occupation number $\bar{n}_j = (e^{\hbar\omega_j/kT} - 1)^{-1}$ with frequencies $\{\omega_m, \omega_p\} = \{\omega_K, \omega_C\}$ and the environmental temperature T [2,82]. Considering the low temperature limit ($T \sim 10$ mT), the thermal occupation number $\bar{n}_j$ is safely ignored with the frequency $\omega_j \sim 1.4$ GHz. Then the dissipation of the Kittel mode and the photon mode therefore can be simplified. Then, the master equation turns to

$$\dot{\hat{\rho}}(t) = -i/\hbar[\hat{H}, \hat{\rho}] + \gamma_s\mathcal{D}[\hat{\sigma}_z]\hat{\rho} + \sum_j\Gamma_j\mathcal{D}[\hat{o}_j]\hat{\rho}. \tag{17}$$

In the frame rotating at the individual spin qubit frequency ω_{NV}, the whole Hamiltonian is first transformed to the form as

$$\hat{H} = \hbar\Delta_1\hat{s}_K^\dagger\hat{s}_K + \hbar\Delta_2\hat{a}^\dagger\hat{a} - \hbar g\hat{s}_K\hat{\sigma}^+ - \hbar\lambda\hat{s}_K^\dagger\hat{a} + \text{H.c.}, \tag{18}$$

where $\Delta_1 = \omega_K - \omega_{\text{NV}}$ and $\Delta_2 = \omega_C - \omega_{\text{NV}}$ [40]. In view of the large detuning ($\Delta_1 \gg g, \lambda$), the Kittel mode can be eliminated [83] and we can obtain the effective interaction between the NV center spin qubit and the CPW resonator photon with the following Hamiltonian:

$$\begin{aligned}\hat{H}_{\text{eff}} = \;& \hbar(\Delta_2 - \beta^2\Delta_1)\hat{a}^\dagger\hat{a} - \tfrac{1}{2}\hbar\alpha^2\Delta_1\hat{\sigma}_z \\ & - \hbar g_{\text{eff}}(\hat{a}^\dagger\hat{\sigma}^- + \text{H.c.}),\end{aligned} \tag{19}$$
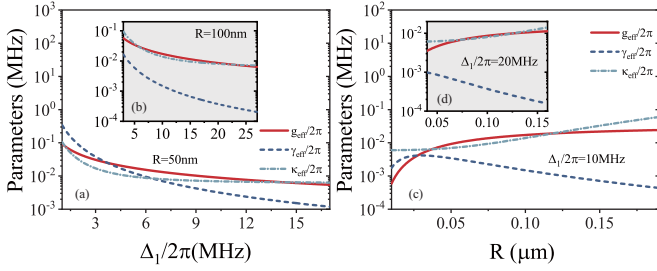
FIG. 3. The effective coupling strength $g_{\text{eff}}/2\pi$ and the effective decay rates $\gamma_{\text{eff}}/2\pi$ and $\kappa_{\text{eff}}/2\pi$ depend on the detuning $\Delta_1/2\pi$ with the value of (a) $R = 50$ nm and (b) $R = 100$ nm, and Inversely these parameters depend on the radius of the micromagnet sphere R with the value of (c) $\Delta_1/2\pi = 10$ MHz and (d) $\Delta_1 = 20$ MHz. We chose the distance between the spin qubit and the surface of the magnetic microsphere as $d = 30$ nm in these figures.

where we defined the dimensionless parameters as $\alpha = g/\Delta_1$ and $\beta = \lambda/\Delta_1$ as well as the effective coupling strength $g_{\text{eff}} = g\lambda/\Delta_1$. This result shows that the interface between the spin and the cavity photon is achieved via utilizing the Kittel mode in the micromagnet as a medium.

We next discuss the effective coupled system with realistic consideration. First, the dissipative interaction system can be described with a reduced effective master equation as

$$\frac{d\hat{\rho}_r(t)}{dt} = -\frac{i}{\hbar}[\hat{H}_{\text{eff}}, \hat{\rho}_r] + \gamma_s \mathcal{D}[\hat{\sigma}_z]\hat{\rho}_r + \gamma_{\text{eff}}\mathcal{D}[\hat{\sigma}_-]\hat{\rho}_r + \kappa_{\text{eff}}\mathcal{D}[\hat{a}]\hat{\rho}_r, \quad (20)$$

where $\gamma_{\text{eff}} = \alpha^2 \gamma_m$ and $\kappa_{\text{eff}} = \kappa + \beta^2 \gamma_m$ are the effective decay rates, respectively. Here, the original dissipation rates are chosen as $\gamma_s/2\pi \sim 1$ kHz [78], $\gamma_m/2\pi \sim 1$ MHz [82], and $\kappa/2\pi \sim 6$ kHz [2]. Taking $\alpha \sim \beta \sim 0.1$ in order to eliminate the Kittel mode, we therefore estimate the effective decay rates as $\gamma_{\text{eff}} \sim 10$ kHz and $\kappa_{\text{eff}} \sim 16$ kHz. Since the spin dephasing rate γ_s is much smaller than the effective decay rates γ_{eff} and κ_{eff}, its effect on the dynamics of the system can be neglected. At the same time, the effective coupling strength g_{eff} can be approximatively obtained as $g_{\text{eff}} \sim 0.1g$, which is larger than the effective decay rates γ_{eff} and κ_{eff}. Therefore, we can obtain the center result of this work: the individual NV center spin qubit can strongly couple to the microwave photon in a CPW resonator under the proper conditions. The spin-photon coupling is well within the strong coupling regime.

We show that the effective coupling strength and decay rates depend on the detuning Δ_1 and the geometrical radius of the magnetic sphere R in Fig. 3. The effective coupling rate $g_{\text{eff}}/2\pi$ and the decay rate $\kappa_{\text{eff}}/2\pi$ increase with the increase of the detuning $\Delta_1/2\pi$, while they decrease with the increase of R. Another effective decay rate $\gamma_{\text{eff}}/2\pi$ decreases with the increase of $\Delta_1/2\pi$ and R. There is always a large range where the effective coupling strength exceeds both the effective decay rates with various values of detuning $\Delta_1/2\pi$ and R. Thus, we can take the effective spin-photon system into the strong coupling regime via tuning the relevant parameters.

In order to compare the effective coupling strength with the effective decay rates, we employ three parameters: $g_{\text{eff}}/\gamma_{\text{eff}}$, $g_{\text{eff}}/\kappa_{\text{eff}}$, and the cooperativity $\mathcal{C} = g_{\text{eff}}^2/\gamma_{\text{eff}}\kappa_{\text{eff}}$. As shown in
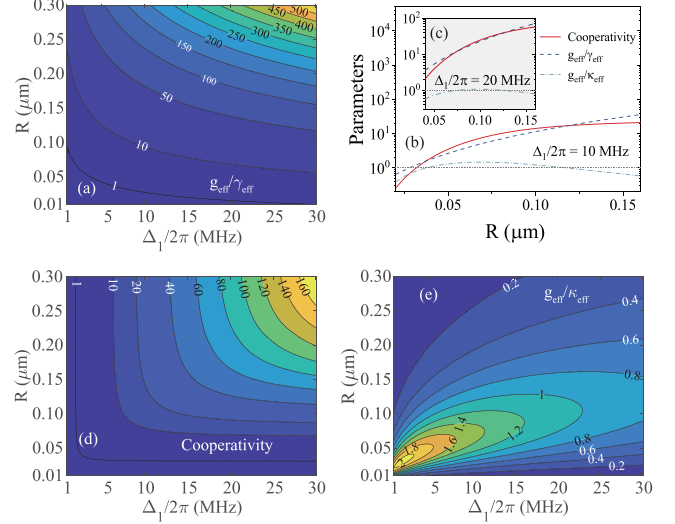

FIG. 4. (a) The contour map of the parameter $g_{\text{eff}}/\gamma_{\text{eff}}$ as a function of the detuning $\Delta_1/2\pi$ and the radius R. (b) and (c) Cooperativity, $g_{\text{eff}}/\gamma_{\text{eff}}$, and $g_{\text{eff}}/\kappa_{\text{eff}}$ versus the radius R under a certain detuning. (d) and (e) The contour maps of the parameters, cooperativity and $g_{\text{eff}}/\kappa_{\text{eff}}$, versus the detuning and the radius. The distance between the spin qubit and the surface of the magnetic microsphere is chosen as $d = 30$ nm.

Fig. 4(a), the parameter $g_{\text{eff}}/\gamma_{\text{eff}}$ increases when the detuning Δ_1 and the radius R become larger. The results show that larger physical dimensions of the magnetic microsphere will allow for stronger effective interaction between the spin qubit and the CPW resonator photon. In Figs. 4(b) and 4(c), we show that the three parameters can be larger than 1 when the radius R is within a certain range. Figure 4(d) shows that the cooperativity $\mathcal{C}$ increases with the increase of the detuning Δ_1 and the radius R, and there is a very large range where the cooperativity even exceeds 10. There is also a range for the parameter $g_{\text{eff}}/\kappa_{\text{eff}} > 1$, as shown in Fig. 4(e). Note that the results displayed in Figs. 3 and 4 are obtained when the NV spin qubit is close to the magnetic microsphere ($d = 30$ nm).

We now explain the significance of the magnetic microsphere in this spin-photon-coupled system using the numerical simulation. The direct interaction between the individual spin qubit and the single photon is very weak on account of the low magnetic effect generated by a single microwave photon. Nevertheless, the magnon mode is sensitive to weak magnetic fields. At the same time, individual spin qubits can strongly couple to the magnon mode with a small distance apart from the magnetic microsphere. Hence, the magnons play a pivotal role in the realization of strong spin-photon coupling. The effective interaction can be proportionally enhanced with the increase of the volume of the magnetic microsphere within a certain range.

We numerically simulate the time evolution of the occupations of the spin qubit, the Kittel magnon, and the CPW resonator using the QUTIP package in PYTHON [84] as shown in the Fig. 5. The damped oscillations of the occupations of the spin and the photon in Fig. 5(a) show the strong coupling between them in the presence of magnons. While in the absence of magnons, Fig. 5(b) shows an exponential decay
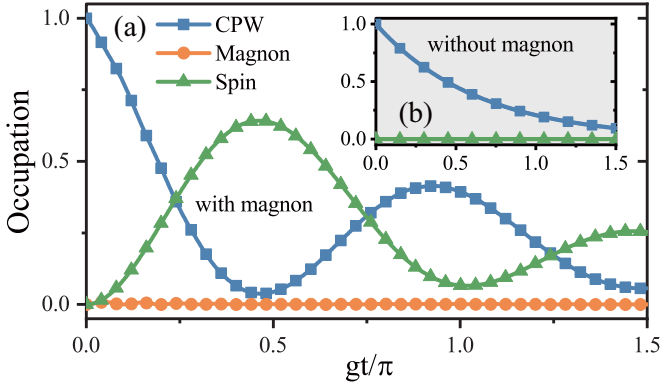
FIG. 5. (a) The occupation map of the three parts in the system depends on the dimensionless time gt/π with the parameters $\gamma_m \sim g$, $\gamma_s \sim 0.1g$, $\kappa \sim 0.5g$, $g \sim \lambda$, and $\Delta_1 \sim 10g$. Panel (b) shows the direct interaction between the spin qubit and the CPW resonator photon without the magnon mode as an intermediary.

curve without oscillations. This result confirms the validity of the effective master equation (20). Note that the population of the virtually excited Kittel mode is nearly zero in the whole process. These results clearly show the significant role played by the magnon in realizing the strong coupling between the spin and the photon.

IV. CONCLUSION

In conclusion, we have proposed a scheme for strongly coupling a single solid-state spin like NV centers to the microwave photons in a CPW cavity via a magnetic microsphere. We have shown that the strong coupling at the single quantum level can be realized by virtual magnonic excitations of a nearby micromagnet. In contrast to the case in the absence of the micromagnet, the spin-photon coupling strength has been enhanced up to typically 4 orders of magnitude. Here, the employment of magnons opens up intriguing perspectives for magnonics and spintronics as well. This regime may facilitate much more powerful applications in quantum information processing based on strongly coupled solid-state spin-photonic systems.

APPENDIX A: QUANTIZATION OF THE SPIN WAVE

In this Appendix, we integrally show the quantization of the spin wave and obtain the theoretical model of the magnon in a ferromagnetic microsphere. First, in Appendix A 1, we introduce the original equation of motion for the magnetization, the general Landau-Lifshitz equation, which is simplified under several physical approximations. Then, we present the Walker mode in a ferrite sphere in Appendix A 2. Based on the magnetostatic energy density expression, we obtain the

intrinsic Hamiltonian and quantization of the magnon modes in Appendix A 3.

1. Spin-wave equations in a magnetic sphere

First, we consider the spin waves with a continuous magnetization field, $\vec{M}(\vec{r}, t)$, and the corresponding electromagnetic field intensities $\vec{E}(\vec{r}, t)$ and $\vec{H}(\vec{r}, t)$. The dynamics of spin waves generally follows the Maxwell's equations with the relationship between the induced magnetization and the applied field. Now we start from the phenomenological Landau-Lifshitz equation of motion for the magnetization [44,85,86]:

$$\frac{d}{dt}\vec{M}(\vec{r}, t) = -|\gamma|\mu_0 \vec{M}(\vec{r}, t) \times \vec{H}_{\text{eff}}(\vec{M}, \vec{r}, t), \quad (A1)$$

where the effective field $\vec{H}_{\text{eff}}(\vec{M}, \vec{r}, t)$ comprises the Maxwellian field $\vec{H}(\vec{r}, t)$ and the extra parts $\vec{H}'(\vec{M}, \vec{r}, t) = \vec{H}_{\text{ex}} + \vec{H}_{\text{an}} + \vec{H}_{\text{dm}}$ [44]. Here, $\vec{H}_{\text{ex}}$, $\vec{H}_{\text{an}}$, and $\vec{H}_{\text{dm}}$, depending on $\vec{M}$, $\vec{r}$, and t, are effective fields due to exchange, anisotropy, and demagnetization induced by the magnetic dipole-dipole interactions, respectively. This means that the Landau-Lifshitz equation is inhomogeneous.

We then assume that the magnet is in the saturated magnetic state along the z axis ($\vec{e}_z$) under the collinear field. Then the fluctuation of the magnetization and the field is very small compared with the constant part [58]. Naturally, they are written as $\vec{M}(\vec{r}, t) = M_S \vec{e}_z + \vec{m}(\vec{r}, t)$ and $\vec{H}(\vec{r}, t) = H_0 \vec{e}_z + \vec{h}(\vec{r}, t)$. Here, $\vec{m} \ll M_S$ and $\vec{h} \ll H_0$ are the dynamical variables to be solved. The exchange field is associated with the domain wall interaction, which is less than the dipole-dipole interaction when the micromagnet size is large compared with the domain wall length. The magnetocrystalline anisotropy for a cubic material is also negligible [44,74,85]. As for the demagnetizing field, we assume $\vec{H}_{\text{dm}} = -(M_S/3)\vec{e}_z$, which is suitable for a spherical magnet [85,87]. The above expressions combined with Eq. (A1) lead to a more clear form of the Landau-Lifshitz equation as

$$\frac{\dot{\vec{m}}(\vec{r}, t)}{|\gamma|\mu_0 M_S H_0} - \vec{e}_z \times \left[\frac{\vec{m}(\vec{r}, t)}{M_S} - \frac{\vec{h}(\vec{r}, t)}{H_0}\right] + \left[\vec{e}_z + \frac{\vec{m}(\vec{r}, t)}{M_S}\right]$$
$$\times \frac{(H_0 - M_S/3)\vec{e}_z}{H_0} = \frac{\vec{h}(\vec{r}, t)}{H_0} \times \frac{\vec{m}(\vec{r}, t)}{M_S}. \quad (A2)$$

Note that the variables $\vec{m}/M_S$ and $\vec{h}/H_0$ are small. Thus, we can safely neglect the second-order term in the above equation. Then the Landau-Lifshitz equation is linearized as [44]

$$\begin{bmatrix} \dot{m}_x(\vec{r}, t) \\ \dot{m}_y(\vec{r}, t) \end{bmatrix} = \begin{bmatrix} -\omega_0 m_y(\vec{r}, t) + \omega_M h_y(\vec{r}, t) \\ \omega_0 m_x(\vec{r}, t) - \omega_M h_x(\vec{r}, t) \end{bmatrix}. \quad (A3)$$

Here, the two relevant system frequencies are $\omega_M = |\gamma|\mu_0 M_S$ and $\omega_0 = |\gamma|\mu_0(H_0 - M_S/3)$.

Finally, it comes to the magnetostatic approximation $\nabla \times \vec{h}(\vec{r}, t) \simeq 0$. In the Maxwell equations, the electric field of the spin wave is uncoupled from $\vec{h}$ under this circumstance. In addition, the approximation makes it easy to introduce the magnetostatic potential through $\vec{h}(\vec{r}, t) = -\nabla\psi(\vec{r}, t)$. Combined with the zero-divergence condition

$\nabla \cdot \vec{b} = 0$ in Maxwell equations, the relation $\vec{b} = \mu_0(\vec{h} + \vec{m})$ allows one to obtain the following equation for three scalar fields (ψ, m_x, m_y) [44]:

$$\nabla^2 \psi(\vec{r}, t) = \partial_x m_x(\vec{r}, t) + \partial_y m_y(\vec{r}, t), \quad \text{(A4)}$$

which is the constraint inside the micromagnet. While the equation outside the micromagnet is $\nabla^2 \psi = 0$. Therefore, the linear scalar equations, Eqs. (A3) and (A4), completely describe the spin wave with the boundary conditions, which is the continuity of the normal direction components of $\vec{h}$ and $\vec{b}$, respectively. The spin-wave eigenmodes solved from these equations are the magnetostatic dipolar spin waves or Walker modes [44,85].

2. Walker modes and Kittel modes

This section reveals the process of calculating the Walker modes. We start from the expressions of the magnetization and magnetic fields in terms of the eigenmodes:

$$\vec{m}(\vec{r}, t) = \sum_\beta [s_\beta \vec{m}_\beta(\vec{r}) e^{-i\omega_\beta t} + \text{c.c.}], \quad \text{(A5a)}$$

$$\vec{h}(\vec{r}, t) = \sum_\beta [s_\beta \vec{h}_\beta(\vec{r}) e^{-i\omega_\beta t} + \text{c.c.}]. \quad \text{(A5b)}$$

Here, the eigenmode fields $\vec{m}_\beta(\vec{r})$ and $\vec{h}_\beta(\vec{r}) = -\nabla \psi_\beta(\vec{r})$ are characterized by a series of mode indices, $\{\beta\}$; an eigenfrequency, ω_β; and a complex amplitude, s_β [88,89]. Then the linearized Landau-Lifshitz equations turn to $i\omega m_x(\vec{r}) = \omega_M \partial_y \psi(\vec{r}) + \omega_0 m_y(\vec{r})$ and $i\omega m_y(\vec{r}) = -\omega_M \partial_x \psi(\vec{r}) - \omega_0 m_x(\vec{r})$, which are time independent. We can eliminate the scalar field $m_x(\vec{r})$ and $m_y(\vec{r})$ through these equations and Eq. (A4). The formula merely contains the magnetostatic potential as

$$\nabla^2 \psi_{\text{out}}(\vec{r}) = 0, \quad \text{(A6a)}$$

$$(1 + \chi_P)\left(\frac{\partial^2}{\partial x^2} + \frac{\partial^2}{\partial y^2}\right)\psi_{\text{in}}(\vec{r}) + \frac{\partial^2}{\partial z^2}\psi_{\text{in}}(\vec{r}) = 0, \quad \text{(A6b)}$$

where ψ_{in} and ψ_{out} are the magnetostatic potentials inside and outside the micromagnet, respectively. Here, the diagonal element of the Polder susceptibility tensor [44] is defined as $\chi_P(\omega) \equiv \omega_M \omega_0 / (\omega_0^2 - \omega^2)$.

As for the outside situation, the general solution in the spherical coordinates is given by

$$\psi_{\text{out}}(\vec{r}) = \sum_{lm}\left[\frac{A_{lm}}{r^{l+1}} + B_{lm}r^l\right]Y_l^m(\theta, \phi). \quad \text{(A7)}$$

Here, A_{lm} and B_{lm} are determined by the boundary conditions and $Y_l^m(\theta, \phi)$ is the spherical harmonics. To solve the potential, a set of nonorthogonal coordinates $\{\xi, \eta, \phi\}$ is introduced. They fulfill $x = \sqrt{\chi_P}R\sqrt{\xi^2 - 1}\sin\eta\cos\phi$, $y = \sqrt{\chi_P}R\sqrt{\xi^2 - 1}\sin\eta\sin\phi$, and $z = \sqrt{\chi_P/(1 + \chi_P)}R\xi\cos\eta$. Thus, the solution of Eq. (A6b) becomes available, which is an expression including Legendre polynomials and spherical harmonics [88,89], as

$$\psi_{\text{in}}(\vec{r}) = \sum_{lm}C_{lm}P_l^m(\xi)Y_l^m(\eta, \phi). \quad \text{(A8)}$$

In each term of the summation, C_{lm} depends on the boundary conditions.

We then determine all the coefficients by the boundary conditions. First, the term corresponding to B_{lm} is not convergent at infinity, which should be removed to make the potential ψ regular. That indicates the first condition, $B_{lm} = 0$. Considering the potential on the surface of the sphere, the coordinates are $\xi \to \xi_0 = \sqrt{(1 + \chi_p)/\chi_p}$ and $\{\eta, \phi\} \to \{\theta, \phi\}$. Applying these coordinates to the two solution expressions, Eq. (A7) and Eq. (A8), we can have the normal-direction-component continuity of $\vec{h}$ and obtain the second condition

$$A_{lm} = C_{lm}P_l^m(\xi_0)R^{l+1}. \quad \text{(A9)}$$

Similarly, we can apply the continuity of the normal component of the $\vec{b}$ field to obtain the final condition

$$\left.\frac{\partial\psi_{\text{out}}}{\partial r}\right|_{r=R} = \frac{\xi_0}{R}\left.\frac{\partial\psi_{\text{in}}}{\partial\xi}\right|_{r=R} - i\frac{\kappa_p}{R}\left.\frac{\partial\psi_{\text{in}}}{\partial\phi}\right|_{r=R}. \quad \text{(A10)}$$

Here, $\kappa_p(\omega) = \omega_M\omega/(\omega_0^2 - \omega^2)$ is the off-diagonal element of the Polder susceptibility tensor [44]. Applying the above fomula and Eq. (A9), the Walker mode eigenfrequency fulfill the equation as [88,89]

$$\xi_0(\omega)\frac{P_l'^m(\xi_0(\omega))}{P_l^m(\xi_0(\omega))} + m\kappa_p(\omega) + l + 1 = 0. \quad \text{(A11)}$$

We can use the indices $\{l, m, n\}$ to mark the nth eigenmodes of the spin waves. The mode functions have been explicitly calculated (Ref. [88]).

3. The intrinsic Hamiltonian and quantization of the magnetostatic dipolar magnon modes

We now show the quantization of the Walker modes from a phenomenological micromagnetic energy functional [58]:

$$E_m(\{\vec{m}\}, \{\vec{h}\}) = \frac{\mu_0}{2}\int dV \vec{m}(\vec{r}, t) \cdot \left[\frac{H_I}{M_S}\vec{m}(\vec{r}, t) - \vec{h}(\vec{r}, t)\right]. \quad \text{(A12)}$$

For convenience, we apply Eq. (A3) to the above expression and the energy becomes $E_m(\{\vec{m}\}) = 1/(2|\gamma|M_S) \int dV(m_x\partial_t m_y - m_y\partial_t m_x)$. Then making use of Eq. (A5a), we transform the energy expression to $E_m = 1/(2\hbar|\gamma|M_S) \sum_\beta \hbar\omega_\beta \Lambda_\beta(s_\beta s_\beta^* + s_\beta^* s_\beta)$, with $\Lambda_\beta = 2\text{Im}\int dV m_{\beta y}m_{\beta x}^*$ [90,91]. Compared with the Hamiltonian of the harmonic oscillator, we can choose adequate eigenmode normalization to fulfill $\Lambda_\beta = M_S|\gamma|\hbar$. After replacing the expansion coefficients with the bosonic magnon operators, i.e., $\{s_\beta, s_\beta^*\} \to \{\hat{s}_\beta, \hat{s}_\beta^\dagger\}$ with the commutation relation $[\hat{s}_\beta, \hat{s}_\beta^\dagger] = 1$, we can obtain the quantized Hamiltonian $\hat{H}_m = \sum_\beta \hbar\omega_\beta[\hat{s}_\beta^\dagger\hat{s}_\beta + 1/2]$, where the constant term is the analog of the zero-point energy.

For simplicity, after defining a zero-point magnetization $M_{0\beta} = \sqrt{\hbar|\gamma|M_S/\tilde{\Lambda}_\beta}$ and the normalization constant $\tilde{\Lambda}_\beta = 2\text{Im}\int dV\tilde{m}_x^*\tilde{m}_y$, the mode functions are replaced as $\{\vec{m}_\beta, \vec{h}_\beta\} \to M_{0\beta}\{\tilde{\vec{m}}_\beta, \tilde{\vec{h}}_\beta\}$. The corresponding magnetization and magnetic field operators are written as $\hat{\vec{m}} = \sum_\beta M_{0\beta}(\tilde{\vec{m}}_\beta\hat{s}_\beta + \text{H.c.})$ and $\hat{\vec{h}} = \sum_\beta M_{0\beta}(\tilde{\vec{h}}_\beta\hat{s}_\beta + \text{H.c.})$.

As for the Kittel mode, especially, the mode function is $\tilde{m}_K = \vec{e}_x + i\vec{e}_y$ with the coordinate vector $\vec{e}_x$ and $\vec{e}_y$. The zero-point magnetization is $M_K = \sqrt{\hbar|\gamma|M_S/2V}$ with the saturation magnetization M_S and the volume V [58]. The corresponding magnetization operator is

$$\hat{\vec{M}} = M_K(\tilde{m}_K \hat{s}_K + \tilde{m}_K^* \hat{s}_K^\dagger). \tag{A13}$$

APPENDIX B: QUANTIZATION OF THE MAGNETIC FIELD GENERATED BY A MAGNETIC SPHERE AND THE INTERACTION HAMILTONIAN

In this Appendix, we show the quantization of the magnetic field generated by a magnetic sphere concretely.

We start from the classical electromagnetism result that the field of a magnetic sphere with magnetization $\vec{M}$ can be described by

$$\vec{B}(\vec{r}) = \frac{\mu_0}{3}\frac{R^3}{r^3}\left[\frac{3(\vec{M}\cdot\vec{r})\vec{r}}{r^2} - \vec{M}\right], \tag{B1}$$

where $\vec{B}(\vec{r})$ is the magnetic field at $\vec{r} = r\cos\theta\,\vec{e}_x + r\sin\theta\,\vec{e}_y$. We then introduce the quantized magnetization operator from Eq. (A13), i.e.,

$$\hat{\vec{M}} = M_K[(\hat{s}_K + \hat{s}_K^\dagger)\vec{e}_x + i(\hat{s}_K - \hat{s}_K^\dagger)\vec{e}_y]. \tag{B2}$$

Applying the above expression to Eq. (B1), we can obtain the operator expression of the magnetic field as

$$\hat{\vec{B}}_m(\vec{r}) = \frac{\mu_0 R^3 M_K}{3r^3}\left\{\left[\left(3C_\theta^2 - 1\right)\hat{X} + 3S_\theta C_\theta \hat{P}\right]\vec{e}_x \right.$$
$$\left. + \left[3S_\theta C_\theta \hat{X} + \left(3S_\theta^2 - 1\right)\hat{P}\right]\vec{e}_y\right\}, \tag{B3}$$

where we define $C_\theta = \cos\theta$, $S_\theta = \sin\theta$, $\hat{X} = \hat{s}_K + \hat{s}_K^\dagger$, and $\hat{P} = i(\hat{s}_K - \hat{s}_K^\dagger)$ for convenience.

Then we consider the interaction between the spin and the quantized magnetic field described by $\hat{H}_{N-K} = (-g_e\mu_B/\hbar)\hat{\vec{B}}\cdot\hat{\vec{S}}$, with the spin operator $\hat{S} = \hat{S}_x\vec{e}_x + \hat{S}_y\vec{e}_y + \hat{S}_z\vec{e}_z$, which leads to the Hamiltonian

$$\hat{H}_{N-K} = -\hbar g\left[\left(3C_\theta^2 - 1\right)(\hat{s}_K + \hat{s}_K^\dagger)(\hat{\sigma}^+ + \hat{\sigma}^-)\right.$$
$$+ 3iS_\theta C_\theta(\hat{s}_K - \hat{s}_K^\dagger)(\hat{\sigma}^+ + \hat{\sigma}^-)$$
$$- 3iS_\theta C_\theta(\hat{s}_K + \hat{s}_K^\dagger)(\hat{\sigma}^+ - \hat{\sigma}^-)$$
$$\left. + \left(3S_\theta^2 - 1\right)(\hat{s}_K - \hat{s}_K^\dagger)(\hat{\sigma}^+ - \hat{\sigma}^-)\right], \tag{B4}$$

where the spin operators are defined as $\hat{\sigma}^\pm = (\hat{S}_x \pm \hat{S}_y)/\hbar$. Under the rotating-wave approximation, the imaginary terms in the second and third lines of the above expression offset with each other, while the left parts can be simplified to the final Hamiltonian $\hat{H}_{N-K} \simeq -\hbar g(\hat{s}_K\hat{\sigma}^+ + \text{H.c.})$. Here, the coupling strength is defined as

$$g = \sqrt{\frac{|\gamma|M_s}{12\pi}}\frac{g_e\mu_0\mu_B R^{3/2}}{(R+d)^3}, \tag{B5}$$

where the distance between the spin qubit and the surface of the magnetic sphere is $d = r - R$ [see Fig. 1(a)].

[1] Z.-L. Xiang, S. Ashhab, J. Q. You, and F. Nori, Hybrid quantum circuits: Superconducting circuits interacting with other quantum systems, Rev. Mod. Phys. **85**, 623 (2013).

[2] P.-B. Li, Y.-C. Liu, S.-Y. Gao, Z.-L. Xiang, P. Rabl, Y.-F. Xiao, and F.-L. Li, Hybrid Quantum Device Based on *NV* Centers in Diamond Nanomechanical Resonators Plus Superconducting Waveguide Cavities, Phys. Rev. Appl. **4**, 044003 (2015).

[3] S. Das, V. E. Elfving, S. Faez, and A. S. Sørensen, Interfacing Superconducting Qubits and Single Optical Photons Using Molecules in Waveguides, Phys. Rev. Lett. **118**, 140501 (2017).

[4] S. Schütz, J. Schachenmayer, D. Hagenmüller, G. K. Brennen, T. Volz, V. Sandoghdar, T. W. Ebbesen, C. Genes, and G. Pupillo, Ensemble-Induced Strong Light-Matter Coupling of a Single Quantum Emitter, Phys. Rev. Lett. **124**, 113602 (2020).

[5] T. Li, Z. Wang, and K. Xia, Multipartite quantum entanglement creation for distant stationary systems, Opt. Express **28**, 1316 (2020).

[6] Q. Bin, X.-Y. Lü, F. P. Laussy, F. Nori, and Y. Wu, *n*-Phonon Bundle Emission via the Stokes Process, Phys. Rev. Lett. **124**, 053601 (2020).

[7] Y. Kubo, C. Grezes, A. Dewes, T. Umeda, J. Isoya, H. Sumiya, N. Morishita, H. Abe, S. Onoda, T. Ohshima, V. Jacques, A. Dréau, J.-F. Roch, I. Diniz, A. Auffeves, D. Vion, D. Esteve, and P. Bertet, Hybrid Quantum Circuit with a Superconducting Qubit Coupled to a Spin Ensemble, Phys. Rev. Lett. **107**, 220501 (2011).

[8] A. Faraon, C. Santori, Z. Huang, V. M. Acosta, and R. G. Beausoleil, Coupling of Nitrogen-Vacancy Centers to Photonic Crystal Cavities in Monocrystalline Diamond, Phys. Rev. Lett. **109**, 033604 (2012).

[9] S. D. Bennett, N. Y. Yao, J. Otterbach, P. Zoller, P. Rabl, and M. D. Lukin, Phonon-Induced Spin-Spin Interactions in Diamond Nanostructures: Application to Spin Squeezing, Phys. Rev. Lett. **110**, 156402 (2013).

[10] P.-B. Li, Z.-L. Xiang, P. Rabl, and F. Nori, Hybrid Quantum Device with Nitrogen-Vacancy Centers in Diamond Coupled to Carbon Nanotubes, Phys. Rev. Lett. **117**, 015502 (2016).

[11] P.-B. Li and F. Nori, Hybrid Quantum System with Nitrogen-Vacancy Centers in Diamond Coupled to Surface-Phonon Polaritons in Piezomagnetic Superlattices, Phys. Rev. Appl. **10**, 024011 (2018).

[12] X.-X. Li, B. Li, and P.-B. Li, Simulation of topological phases with color center arrays in phononic crystals, Phys. Rev. Research **2**, 013121 (2020).

[13] A. Blais, S. M. Girvin, and W. D. Oliver, Quantum information processing and quantum optics with circuit quantum electrodynamics, Nat. Phys. **16**, 247 (2020).

[14] X.-X. Li, P.-B. Li, H.-R. Li, H. Gao, and F.-L. Li, Simulation of topological Zak phase in spin-phononic crystal networks, Phys. Rev. Research **3**, 013025 (2021).

[15] O. Arcizet, V. Jacques, A. Siria, P. Poncharal, P. Vincent, and S. Seidelin, A single nitrogen-vacancy defect coupled to a nanomechanical oscillator, Nat. Phys. **7**, 879 (2011).

[16] P.-B. Li, Y. Zhou, W.-B. Gao, and F. Nori, Enhancing Spin-Phonon and Spin-Spin Interactions Using Linear Resources in a Hybrid Quantum System, Phys. Rev. Lett. **125**, 153602 (2020).

[17] J. Twamley and S. D. Barrett, Superconducting cavity bus for single nitrogen-vacancy defect centers in diamond, Phys. Rev. B **81**, 241202(R) (2010).

[18] R. Amsüss, C. Koller, T. Nöbauer, S. Putz, S. Rotter, K. Sandner, S. Schneider, M. Schramböck, G. Steinhauser, H. Ritsch, J. Schmiedmayer, and J. Majer, Cavity QED with Magnetically Coupled Collective Spin States, Phys. Rev. Lett. **107**, 060502 (2011).

[19] V. L. Grigoryan, K. Shen, and K. Xia, Synchronized spin-photon coupling in a microwave cavity, Phys. Rev. B **98**, 024406 (2018).

[20] B. Julsgaard, C. Grezes, P. Bertet, and K. Mølmer, Quantum Memory for Microwave Photons in an Inhomogeneously Broadened Spin Ensemble, Phys. Rev. Lett. **110**, 250503 (2013).

[21] A. Imamoğlu, Cavity QED Based on Collective Magnetic Dipole Coupling: Spin Ensembles as Hybrid Two-Level Systems, Phys. Rev. Lett. **102**, 083602 (2009).

[22] Y. Kubo, F. R. Ong, P. Bertet, D. Vion, V. Jacques, D. Zheng, A. Dréau, J.-F. Roch, A. Auffeves, F. Jelezko, J. Wrachtrup, M. F. Barthe, P. Bergonzo, and D. Esteve, Strong Coupling of a Spin Ensemble to a Superconducting Resonator, Phys. Rev. Lett. **105**, 140502 (2010).

[23] A. Reiserer and G. Rempe, Cavity-based quantum networks with single atoms and optical photons, Rev. Mod. Phys. **87**, 1379 (2015).

[24] A. Galindo and M. A. Martín-Delgado, Information and computation: Classical and quantum aspects, Rev. Mod. Phys. **74**, 347 (2002).

[25] C. L. Degen, F. Reinhard, and P. Cappellaro, Quantum sensing, Rev. Mod. Phys. **89**, 035002 (2017).

[26] G. D. Fuchs, G. Burkard, P. V. Klimov, and D. D. Awschalom, A quantum memory intrinsic to single nitrogen–vacancy centres in diamond, Nat. Phys. **7**, 789 (2011).

[27] H.-S. Zhong, H. Wang, Y.-H. Deng, M.-C. Chen, L.-C. Peng, Y.-H. Luo, J. Qin, D. Wu, X. Ding, Y. Hu, P. Hu, X.-Y. Yang, W.-J. Zhang, H. Li, Y. Li, X. Jiang, L. Gan, G. Yang, L. You, Z. Wang, L. Li, N.-L. Liu, C.-Y. Lu, and J.-W. Pan, Quantum computational advantage using photons, Science **370**, 1460 (2020).

[28] X. Mi, M. Benito, S. Putz, D. M. Zajac, J. M. Taylor, G. Burkard, and J. R. Petta, A coherent spin–photon interface in silicon, Nature (London) **555**, 599 (2018).

[29] D. D. Awschalom, R. Hanson, J. Wrachtrup, and B. B. Zhou, Quantum technologies with optically interfaced solid-state spins, Nat. Photon. **12**, 516 (2018).

[30] I. Aharonovich, A. D. Greentree, and S. Prawer, Diamond photon., Nat. Photonics **5**, 397 (2011).

[31] D. Lee, K. W. Lee, J. V. Cady, P. Ovartchaiyapong, and A. C. B. Jayich, Topical review: Spins and mechanics in diamond, J. Opt. **19**, 033001 (2017).

[32] W. D. Marcus, B. M. Neil, D. Paul, J. Fedor, W. Jörg, and C. L. H. Lloyd, The nitrogen-vacancy color center in diamond, Phys. Rep. **528**, 1 (2013).

[33] M. W. Doherty, V. V. Struzhkin, D. A. Simpson, L. P. McGuinness, Y. Meng, A. Stacey, T. J. Karle, R. J. Hemley, N. B. Manson, L. C. L. Hollenberg, and S. Prawer, Electronic Properties and Metrology Applications of the Diamond NV⁻ Center under Pressure, Phys. Rev. Lett. **112**, 047601 (2014).

[34] J. F. Barry, J. M. Schloss, E. Bauch, M. J. Turner, C. A. Hart, L. M. Pham, and R. L. Walsworth, Sensitivity optimization for NV-diamond magnetometry, Rev. Mod. Phys. **92**, 015004 (2020).

[35] N. Bar-Gill, L. M. Pham, A. Jarmola, D. Budker, and R. L. Walsworth, Solid-state electronic spin coherence time approaching one second, Nat. Commun. **4**, 1743 (2013).

[36] M. H. Abobeih, J. Cramer, M. A. Bakker, N. Kalb, M. Markham, D. J. Twitchen, and T. H. Taminiau, One-second coherence for a single electron spin coupled to a multi-qubit nuclear-spin environment, Nat. Commun. **9**, 2552 (2018).

[37] F. Dolde, H. Fedder, M. W. Doherty, T. Nöbauer, F. Rempp, G. Balasubramanian, T. Wolf, F. Reinhard, L. C. L. Hollenberg, F. Jelezko, and J. Wrachtrup, Electric-field sensing using single diamond spins, Nat. Phys. **7**, 459 (2011).

[38] S. Kolkowitz, J. A. C. Bleszynski, Q. P. Unterreithmeier, S. D. Bennett, P. Rabl, J. G. E. Harris, and M. D. Lukin, Coherent sensing of a mechanical resonator with a single-spin qubit, Science **335**, 1603 (2012).

[39] D. Roy, C. M. Wilson, and O. Firstenberg, Colloquium: Strongly interacting photons in one-dimensional continuum, Rev. Mod. Phys. **89**, 021001 (2017).

[40] Y.-C. Liu, X. Luan, H.-K. Li, Q. Gong, C. W. Wong, and Y.-F. Xiao, Coherent Polariton Dynamics in Coupled Highly Dissipative Cavities, Phys. Rev. Lett. **112**, 213602 (2014).

[41] J. Verdú, H. Zoubi, C. Koller, J. Majer, H. Ritsch, and J. Schmiedmayer, Strong Magnetic Coupling of an Ultracold Gas to a Superconducting Waveguide Cavity, Phys. Rev. Lett. **103**, 043603 (2009).

[42] P. Rabl, D. DeMille, J. M. Doyle, M. D. Lukin, R. J. Schoelkopf, and P. Zoller, Hybrid Quantum Processors: Molecular Ensembles as Quantum Memory for Solid State Circuits, Phys. Rev. Lett. **97**, 033003 (2006).

[43] D. Zhang, X.-M. Wang, T.-F. Li, X.-Q. Luo, W. Wu, F. Nori, and J. Q. You, Cavity quantum electrodynamics with ferromagnetic magnons in a small yttrium-iron-garnet sphere, npj Quantum Inf. **1**, 15014 (2015).

[44] D. D. Stancil and A. Prabhakar, *Spin Waves: Theory and Applications* (Springer, New York, 2009).

[45] X. Zhang, C.-L. Zou, L. Jiang, and H. X. Tang, Cavity magnomechanics, Sci. Adv. **2**, e1501286 (2016).

[46] J. A. Haigh, A. Nunnenkamp, A. J. Ramsay, and A. J. Ferguson, Triple-Resonant Brillouin Light Scattering in Magneto-Optical Cavities, Phys. Rev. Lett. **117**, 133602 (2016).

[47] D. Lachance-Quirion, Y. Tabuchi, A. Gloppe, K. Usami, and Y. Nakamura, Hybrid quantum systems based on magnonics, Appl. Phys. Express **12**, 070101 (2019).

[48] S. P. Wolski, D. Lachance-Quirion, Y. Tabuchi, S. Kono, A. Noguchi, K. Usami, and Y. Nakamura, Dissipation-Based Quantum Sensing of Magnons with a Superconducting Qubit, Phys. Rev. Lett. **125**, 117701 (2020).

[49] Ö. O. Soykal and M. E. Flatté, Strong Field Interactions between a Nanomagnet and a Photonic Cavity, Phys. Rev. Lett. **104**, 077202 (2010).

[50] Y. Tabuchi, S. Ishino, T. Ishikawa, R. Yamazaki, K. Usami, and Y. Nakamura, Hybridizing Ferromagnetic Magnons and Microwave Photons in the Quantum Limit, Phys. Rev. Lett. **113**, 083603 (2014).

[51] X. Zhang, C.-L. Zou, L. Jiang, and H. X. Tang, Strongly Coupled Magnons and Cavity Microwave Photons, Phys. Rev. Lett. **113**, 156401 (2014).

[52] Y. Tabuchi, S. Ishino, A. Noguchi, T. Ishikawa, R. Yamazaki, K. Usami, and Y. Nakamura, Coherent coupling between a ferromagnetic magnon and a superconducting qubit, Science **349**, 405 (2015).

[53] N. J. Lambert, J. A. Haigh, and A. J. Ferguson, Identification of spin wave modes in yttrium iron garnet strongly coupled to a co-axial cavity, J. Appl. Phys. **117**, 053910 (2015).

[54] N. J. Lambert, J. A. Haigh, S. Langenfeld, A. C. Doherty, and A. J. Ferguson, Cavity-mediated coherent coupling of magnetic moments, Phys. Rev. A **93**, 021803(R) (2016).

[55] J. Bourhill, N. Kostylev, M. Goryachev, D. L. Creedon, and M. E. Tobar, Ultrahigh cooperativity interactions between magnons and resonant photons in a YIG sphere, Phys. Rev. B **93**, 144420 (2016).

[56] N. Kostylev, M. Goryachev, and M. E. Tobar, Superstrong coupling of a microwave cavity to yttrium iron garnet magnons, Appl. Phys. Lett. **108**, 062402 (2016).

[57] Y.-P. Wang, G.-Q. Zhang, D. Zhang, T.-F. Li, C.-M. Hu, and J. Q. You, Bistability of Cavity Magnon Polaritons, Phys. Rev. Lett. **120**, 057202 (2018).

[58] C. Gonzalez-Ballestero, D. Hümmer, J. Gieseler, and O. Romero-Isart, Theory of quantum acoustomagnonics and acoustomechanics with a micromagnet, Phys. Rev. B **101**, 125404 (2020).

[59] J. Gieseler, A. Kabcenell, E. Rosenfeld, J. D. Schaefer, A. Safira, M. J. A. Schuetz, C. Gonzalez-Ballestero, C. C. Rusconi, O. Romero-Isart, and M. D. Lukin, Single-Spin Magnetomechanics with Levitated Micromagnets, Phys. Rev. Lett. **124**, 163604 (2020).

[60] C. W. Sandweg, Y. Kajiwara, A. V. Chumak, A. A. Serga, V. I. Vasyuchka, M. B. Jungfleisch, E. Saitoh, and B. Hillebrands, Spin Pumping by Parametrically Excited Exchange Magnons, Phys. Rev. Lett. **106**, 216601 (2011).

[61] H. Huebl, C. W. Zollitsch, J. Lotze, F. Hocke, M. Greifenstein, A. Marx, R. Gross, and S. T. B. Goennenwein, High Cooperativity in Coupled Microwave Resonator Ferrimagnetic Insulator Hybrids, Phys. Rev. Lett. **111**, 127003 (2013).

[62] X. Zhang, C. Zou, L. Jiang, and H. X. Tang, Superstrong coupling of thin film magnetostatic waves with microwave cavity, J. Appl. Phys. **119**, 023905 (2016).

[63] Y. Li, T. Polakovic, Y.-L. Wang, J. Xu, S. Lendinez, Z. Zhang, J. Ding, T. Khaire, H. Saglam, R. Divan, J. Pearson, W.-K. Kwok, Z. Xiao, V. Novosad, A. Hoffmann, and W. Zhang, Strong Coupling between Magnons and Microwave Photons in On-Chip Ferromagnet-Superconductor Thin-Film Devices, Phys. Rev. Lett. **123**, 107701 (2019).

[64] J. T. Hou and L. Liu, Strong Coupling between Microwave Photons and Nanomagnet Magnons, Phys. Rev. Lett. **123**, 107702 (2019).

[65] H. Wang, J. Chen, T. Liu, J. Zhang, K. Baumgaertl, C. Guo, Y. Li, C. Liu, P. Che, S. Tu, S. Liu, P. Gao, X. Han, D. Yu, M. Wu, D. Grundler, and H. Yu, Chiral Spin-Wave Velocities Induced by All-Garnet Interfacial Dzyaloshinskii-Moriya

[66] X. Zhang, G. E. W. Bauer, and T. Yu, Unidirectional Pumping of Phonons by Magnetization Dynamics, Phys. Rev. Lett. **125**, 077203 (2020).

Interaction in Ultrathin Yttrium Iron Garnet Films, Phys. Rev. Lett. **124**, 027203 (2020).

[67] N. Almulhem, M. Stebliy, J. Portal, A. Samardak, H. Beere, D. Ritchie, and A. Nogaret, Photovoltage detection of spin excitation of a ferromagnetic stripe and disk at low temperature, Jpn. J. Appl. Phys. **59**, SEED02 (2020).

[68] P. Huillery, T. Delord, L. Nicolas, M. Van Den Bossche, M. Perdriat, and G. Hétet, Spin mechanics with levitating ferromagnetic particles, Phys. Rev. B **101**, 134415 (2020).

[69] R. Simons and R. N. Simons, *Coplanar Waveguide Circuits, Components, and Systems* (Wiley Online Library, New York, 2001), Vol. 15.

[70] S. A. Wolf, D. D. Awschalom, R. A. Buhrman, J. M. Daughton, S. von Molnár, M. L. Roukes, A. Y. Chtchelkanova, and D. M. Treger, Spintronics: A spin-based electronics vision for the future, Science **294**, 1488 (2001).

[71] J. H. Wesenberg, A. Ardavan, G. A. D. Briggs, J. J. L. Morton, R. J. Schoelkopf, D. I. Schuster, and K. Mølmer, Quantum Computing with an Electron Spin Ensemble, Phys. Rev. Lett. **103**, 070502 (2009).

[72] Y. Tabuchi, S. Ishino, A. Noguchi, T. Ishikawa, R. Yamazaki, K. Usami, and Y. Nakamura, Quantum magnonics: The magnon meets the superconducting qubit, C. R. Phys. **17**, 729 (2016).

[73] R. G. E. Morris, A. F. van Loo, S. Kosen, and A. D. Karenowska, Strong coupling of magnons in a YIG sphere to photons in a planar superconducting resonator in the quantum limit, Sci. Rep. **7**, 11511 (2017).

[74] H. Maier-Flaig, S. Klingler, C. Dubs, O. Surzhenko, R. Gross, M. Weiler, H. Huebl, and S. T. B. Goennenwein, Temperature-dependent magnetic damping of yttrium iron garnet spheres, Phys. Rev. B **95**, 214423 (2017).

[75] J. Li, S.-Y. Zhu, and G. S. Agarwal, Squeezed states of magnons and phonons in cavity magnomechanics, Phys. Rev. A **99**, 021801(R) (2019).

[76] M. J. Martínez-Pérez and D. Zueco, Strong coupling of a single photon to a magnetic vortex, ACS Photon. **6**, 360 (2019).

[77] J. R. Maze, A. Gali, E. Togan, Y. Chu, A. Trifonov, E. Kaxiras, and M. D. Lukin, Properties of nitrogen-vacancy centers in diamond: The group theoretic approach, New J. Phys. **13**, 025025 (2011).

[78] B. Li, P.-B. Li, Y. Zhou, J. Liu, H.-R. Li, and F.-L. Li, Interfacing a Topological Qubit with a Spin Qubit in a Hybrid Quantum System, Phys. Rev. Appl. **11**, 044026 (2019).

[79] P. Bushev, A. K. Feofanov, H. Rotzinger, I. Protopopov, J. H. Cole, C. M. Wilson, G. Fischer, A. Lukashenko, and A. V. Ustinov, Ultralow-power spectroscopy of a rare-earth spin ensemble using a superconducting resonator, Phys. Rev. B **84**, 060501(R) (2011).

[80] M. Jenkins, T. Hümmer, M. J. Martínez-Pérez, J. García-Ripoll, D. Zueco, and F. Luis, Coupling single-molecule magnets to quantum circuits, New J. Phys. **15**, 095007 (2013).

[81] M. D. Jenkins, U. Naether, M. Ciria, J. Sesé, J. Atkinson, C. Sánchez-Azqueta, E. Barco, J. Majer, D. Zueco, and F. Luis, Nanoscale constrictions in superconducting coplanar waveguide resonators, Appl. Phys. Lett. **105**, 162601 (2014).

[82] C. Gonzalez-Ballestero, J. Gieseler, and O. Romero-Isart, Quantum Acoustomechanics with a Micromagnet, Phys. Rev. Lett. **124**, 093602 (2020).

[83] P.-B. Li, S.-Y. Gao, H.-R. Li, S.-L. Ma, and F.-L. Li, Dissipative preparation of entangled states between two spatially separated nitrogen-vacancy centers, Phys. Rev. A **85**, 042306 (2012).

[84] J. R. Johansson, P. D. Nation, and F. Nori, QuTiP 2: A python framework for the dynamics of open quantum systems, Comput. Phys. Commun. **184**, 1234 (2013).

[85] A. Aharoni, *Introduction to the Theory of Ferromagnetism* (Clarendon Press, Oxford, 2000).

[86] A. G. Gurevich and G. A. Melkov, *Magnetization Oscillations and Waves* (CRC Press, Boca Raton, FL, 1996).

[87] J. D. Jackson, *Classical Electrodynamics* (Wiley & Sons, New York, 2007).

[88] P. C. Fletcher and R. O. Bell, Ferrimagnetic resonance modes in spheres, J. Appl. Phys. **30**, 687 (1959).

[89] P. Röschmann and H. Dötsch, Properties of magnetostatic modes in ferrimagnetic spheroids, Phys. Status Solidi B **82**, 11 (1977).

[90] D. L. Mills, Quantum theory of spin waves in finite samples, J. Magn. Magn. Mater. **306**, 16 (2006).

[91] L. R. Walker, Magnetostatic modes in ferromagnetic resonance, Phys. Rev. **105**, 390 (1957).